Materials Science & Engineering C 81 (2017) 373–379

Contents lists available at ScienceDirect

Materials Science & Engineering C

journal homepage: www.elsevier.com/locate/msec

Biomineralized diamond-like carbon films with incorporated titanium dioxide nanoparticles improved bioactivity properties and reduced biofilm formation

F.S. Lopes[a,b], J.R. Oliveira[c], J. Milani[b], L.D. Oliveira[c], J.P.B. Machado[d], V.J. Trava-Airoldi[d], A.O. Lobo[a,b,e,f,g], F.R. Marciano[a,b,e,f,*]

[a] Laboratory of Biomedical Nanotechnology, Universidade Brasil, 08230-030 Itaquera, São Paulo, Brazil
[b] Laboratory of Biomedical Nanotechnology, Universidade do Vale do Paraiba, São José dos Campos, 12244-000, São Paulo, Brazil
[c] Department of Biosciences and Oral Diagnosis, Institute of Science and Technology, UNESP-Univ Estadual Paulista, São José dos Campos, SP, Brazil
[d] Associated Laboratory of Sensors and Materials, National Institute for Space Research, São José dos Campos, SP, Brazil
[e] Biomaterials Innovation Research Center, Department of Medicine, Brigham and Women's Hospital, Harvard Medical School, Cambridge, MA 02139, USA
[f] Nanomedicine Lab, Department of Chemical Engineering, Northeastern University, Boston, MA 02115, USA
[g] Interdisciplinary Laboratory for Advanced Materials, PPGCM, Technology Center, Federal University of Piaui, 64049-550 Teresina, PI, Brazil

ARTICLE INFO

Keywords:
Diamond-like carbon
Titanium dioxide
Nanoparticles
Biomineralization
Hydroxyapatite
Antibacterial activity

ABSTRACT

Recently, the development of coatings to protect biomedical alloys from oxidation, passivation and to reduce the ability for a bacterial biofilm to form after implantation has emerged. Diamond-like carbon films are commonly used for implanted medical due to their physical and chemical characteristics, showing good interactions with the biological environment. However, these properties can be significantly improved when titanium dioxide nanoparticles are included, especially to enhance the bactericidal properties of the films. So far, the deposition of hydroxyapatite on the film surface has been studied in order to improve biocompatibility and bioactive behavior. Herein, we developed a new route to obtain a homogeneous and crystalline apatite coating on diamond-like carbon films grown on 304 biomedical stainless steel and evaluated its antibacterial effect. For this purpose, films containing two different concentrations of titanium dioxide (0.1 and 0.3 g/L) were obtained by chemical vapor deposition. To obtain the apatite layer, the samples were soaked in simulated body fluid solution for up to 21 days. The antibacterial activity of the films was evaluated by bacterial eradication tests using *Staphylococcus aureus* biofilm. Scanning electron microscopy, X-ray diffraction, Raman scattering spectroscopy, and goniometry showed that homogeneous, crystalline, and hydrophilic apatite films were formed independently of the titanium dioxide concentration. Interestingly, the diamond-like films containing titanium dioxide and hydroxyapatite reduced the biofilm formation compared to controls. A synergism between hydroxyapatite and titanium dioxide that provided an antimicrobial effect against opportunistic pathogens was clearly observed.

1. Introduction

Currently, alternatives are being developed to improve the biological properties of biomedical metal alloys and to reduce the need to administer antibiotics during and after their implantation by surgical procedures. It's known that metal alloys have been used for many years as substitutes for bones and/or to promote bone regeneration after fracture. To solve this, the use of stainless steel for biomedical applications is cheaper and has been extensively used [1–3]. However, several problems have been encountered when stainless steel is implanted at human body [4,5]. To solve these problems, several alternatives have been developed to modify the surface of metal alloys to improve their biocompatibility [6,7]. Contributing to this, the deposition of thin films can be interesting due to the feasibility and reproducibility of their direct deposition on metal alloys.

Diamond-like carbon (DLC) coatings can impart wear resistance, hardness, and corrosion resistance to the surface of a medical device [8–11]. DLC films are mostly obtained by plasma decomposition of a hydrocarbon-rich atmosphere using chemical vapor deposition [8–11]. Commonly, when DLC films are obtained by methane decomposition, a typical sp2-hybridized cluster interconnected with sp3-hybridized carbon atoms is produced. Then, the mechanical properties (e.g. hardness, Young's modulus, adhesion to the substrate, internal stresses) as well as important electronic properties (e.g. optical gap,

* Corresponding author at: Laboratory of Biomedical Nanotechnology, Universidade Brasil, 08230-030 Itaquera, São Paulo, Brazil.
E-mail address: frmarciano@pq.cnpq.br (F.R. Marciano).

http://dx.doi.org/10.1016/j.msec.2017.07.043
Received 11 May 2017; Received in revised form 7 July 2017; Accepted 27 July 2017
Available online 29 July 2017

photoluminescence, and conduction behavior) may be pre-determined to a certain extent by varying the sp3/sp2 bonding ratio [8–11]. These coatings consist of dense amorphous carbon or hydrocarbon and their mechanical properties fall between those of graphite and diamond [8,9]. However, the addition of different elements to the films can easily tune their surface chemical behavior [12].

Titanium is a reactive metal that in air, water, or any electrolyte spontaneously forms a thin native oxide film, which is responsible for the biocompatibility of the titanium [13]. This oxide layer is responsible for the bone-bonding characteristics of titanium implants [14]. Its photo-semiconductor properties enable TiO_2 use as an antibacterial agent for decomposition of organisms [15–18]. However, these properties are strongly dependent on the crystalline structure, morphology, and crystallite size [15].

Many alternatives have been developed to obtain nanoparticles, nanocarriers and thin films for biological applications. In this context, hybrid materials and inorganic materials are upcoming materials for delivery, therapy, sensors, and so on [19–23]. However, the application of TiO_2-DLC films has become of interest and was already reported [24]. Antibacterial tests against *Escherichia coli* showed an increase of DLC bactericidal activity when the amount of TiO_2 was increased. Thorwarth et al. [25] showed that a-C:H layers deposited on TiAl6V4 promoted cell proliferation and differentiation. Amin et al. [26] showed that TiO_2-DLC film presented biomimetic properties. However, the antibacterial properties of biomineralizated-TiO_2-DLC coatings have not yet been studied.

Herein, for the first time, we obtained a new thin film using a simple approach to produce biomineralizated-TiO_2-DLC and its bactericidal properties were also further explored. Interestingly, the apatite-TiO_2-DLC films avoided and reduced biofilm formation by a very common pathogenic agent in a hospital environment. Our alternatives open perspectives for the application of such developed films to improve bone regeneration and to control biofilm formation, allowing the administration of antibiotics to be avoided.

2. Materials and methods

2.1. Deposition and characterization of biomineralized diamond-like carbon films containing titanium dioxide nanoparticles and hydroxyapatite

Discs of 304 stainless steel (diameter of 6 mm and thickness of 1 mm) were used as substrates. DLC and TiO_2-DLC films (0.1 and 0.3 g/L) were produced using plasma-enhanced chemical vapor deposition as already reported [24].

The structural characteristics were analyzed by Raman spectroscopy (Renishaw 2000 system with Ar^+-ions, λ = 514 nm, spot-size = 2.5 μm, and power = ~0.6 mW) with backscattering geometry.

To obtain apatite formation, the different samples were soaked in simulated body fluid (SBF, 5×, Table 1) [27]. The pH of the solution was adjusted to 6.10 using HCl (0.1% v/v) and the media was changed every three days. After the biomineralization period, samples were removed, washed in hot deionized water, dried in an oven at 50 °C for 24 h, and sterilized by autoclave (121 °C/15 min).

Scanning electron microscopy (SEM, EVO MA 10, Zeiss) was used to analyze the apatite produced. Energy dispersive X-ray spectroscopy (EDX) (Inca Penta FET × 3, Oxford Instruments) was used to identify the Ca and P elements after biomineralization. The structural analysis of biological apatites on stainless steel, DLC, and TiO_2-DLC films was performed at room temperature by X-ray diffractometry (XRD) using an X-Pert Philips instrument with Cu Kα radiation (λ = 0.154056 nm) with a 2θ angle of 10° to 50° under the following conditions: voltage of 40 kV, current of 30 mA, step size of 0.02°, and counting time of 2 s per step. The diffraction peaks were indexed according to the Joint Committee on Powder Diffraction Standards (JCPDS) using X'pert HighScore software (www.panalytical.com).

The sessile drop method (Kruss EasyDrop DSA 100) was used to measure the contact angle (θ). Two different liquids (distilled water and diiodomethane) were used for surface energy calculations, following the Owens method [28]. The liquid was dropped automatically by a computer-controlled system. These values were used to calculate the thermodynamic work of adhesion (W_{Ad}) using the standard Young-Dupré relationship [29,30]. All measurements were carried out at room temperature.

Table 1
Quantity of reagents used to prepare SBF.

Reagents	Concentration (g/L)
NaCl	40.0
$MgCl_2$	1.52
$CaCl_2.2H_2O$	1.84
$Na_2HPO_4.2H_2O$	0.89
$NaHCO_3$	1.76

2.2. Bactericidal evaluation of biomineralized diamond-like carbon films containing titanium dioxide nanoparticles and hydroxyapatite

Standard strains of *Staphylococcus aureus* (ATCC 6538) were used to evaluate the antibacterial activity of the biofilm. HAp/stainless steel, HAp/DLC, HAp/TiO_2-DLC (0.1 g/L), and HAp/TiO_2-DLC (0.3 g/L) were used. Firstly, *S. aureus* was cultured in Brain Heart Infusion agar (BHI, Himedia, Mumbai, India) for 24 h at 37 °C. Subsequently, the suspension was centrifuged (2000 rpm/10 min) and the pellet was suspended in sterile saline solution (0.9% NaCl). Then, the turbidity of the solution was adjusted with a spectrophotometer to obtain a concentration of 10^6 CFU/mL (colony forming units per milliliter). Next, we added 1000 μL of BHI, different samples (n = 5), and 100 μL of the standardized suspension of *S. aureus* (using a 24-well plate, 37 °C) and incubated for 24 h. The medium was changed after 24 h. Thus, the biofilm formed on the discs was disaggregated by ultrasonic homogenizer (Sonoplus HD 2200, 50 W, Bandelin Electronic, Berlin, Germany) for 30 s at 25% power. Then, the discs were transferred to plastic tubes containing 10 mL of sterile saline solution and after disaggregation of the biofilm, the microbial suspension was diluted (1:10) and 100 μL of each dilution was seeded on BHI agar in duplicate. After 48 h of incubation, the CFUs were counted and the values were converted to log10. The statistical differences were analyzed by one-way ANOVA (Graph Pad PRISM 6®). The bacterial populations on stainless steel, DLC, and TiO_2-DLC films after biomineralization were obtained with a normal distribution and independently to each experiment. P-values of < 0.05 were considered to indicate statistical differences.

3. Results and discussion

Raman spectra were composed of two broad bands, centered at approximately ~1330 cm^{-1} (D band) and ~1550 cm^{-1} (G band), as already reported by Robertson and Ferrari [31]. The D and G band positions were determined by subtracting a linear background and fitting a Gaussian function to the peak of the Raman spectrum (Fig. 1). Table 2 shows the main parameters obtained through the spectra. The G band is due to the bond stretching of all pairs of sp^2 atoms in both rings and chains. The D band is assigned to breathing modes of sp^2 atoms in rings and appears only in the presence of defects. The TiO_2-DLC films presented a shift in the D and G band positions toward higher wavenumbers due to the presence of defects. Using the full width at half maximum (FWHM) of the G band, it was possible to determine the structural disorder that arises from bond length distortions. The FWHM is small irrespective of whether the clusters are defect free, unstrained, or "molecular". For a given cluster size, a higher bond length and bond angle disorder lead to a higher FWHM (G). This implies that the FWHM (G) is mainly a probe of structural disorder. Higher excitation energies

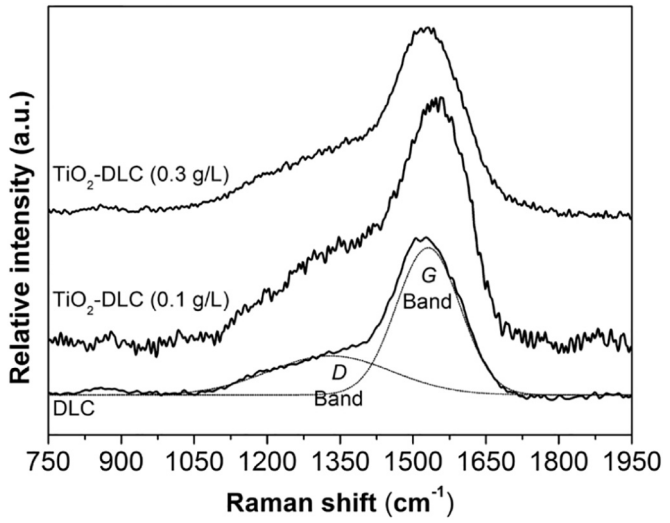

Fig. 1. Raman spectra from as-grown DLC and TiO_2-DLC films. The spectra are vertically shifted for ease of comparison.

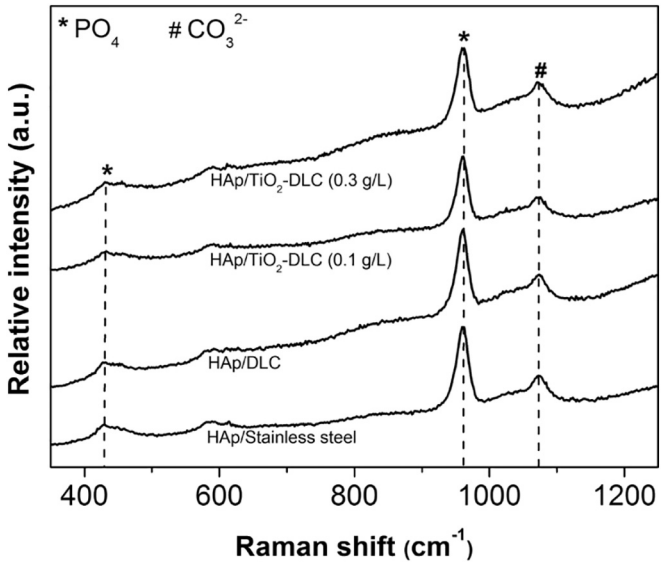

Fig. 2. Raman spectra from HAp obtained on stainless steel, DLC, and TiO_2-DLC films. The spectra are vertically shifted for ease of comparison. $N = 5$.

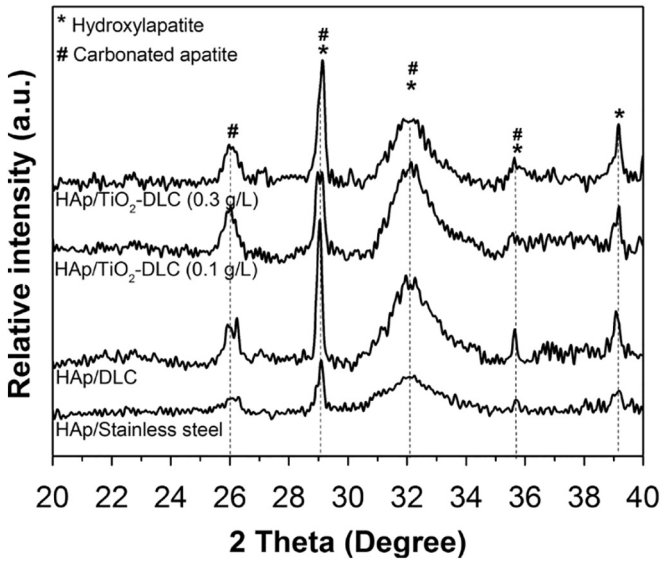

Fig. 3. X-ray diffractograms of apatite grown on stainless steel, DLC, and TiO_2-DLC films. $N = 5$.

are resonant with smaller clusters.

The incorporation of TiO_2 nanoparticles in DLC films results in an increase of the intensity ratio of the *D* and *G* areas (A_D/A_G) and a shift of the *D* and *G* bands toward higher wave numbers. A_D/A_G and $FWHM_D/FWHM_G$ increase as the TiO_2 concentration increases. This can been attributed to the reduction of the number of sp^3 sites, which increases the sp^2/sp^3 ratio [32]. Also, a sudden downward shift was observed after incorporating 0.3 g/L of TiO_2 in the DLC structure. This alteration may act as an interstitial defect due to the presence of either TiO_2 between C—C bounds or a possible alignment of carbon atoms in unit cells. The presence of TiO_2 nanoparticles is responsible for lower internal stress, increasing the amount of the softer graphitic phase [33].

Fig. 2 shows the Raman spectra of biomineralized samples. Briefly, peaks attributed to C—C bonds were not observed due to apatite formation. Clearly, a background occurred in all collected spectra due to the photoluminescence of the apatite films, which is commonly observed when they are excited using a wavelength of 514.5 nm. The sharp band centered at 961 cm^{-1} is characteristic of crystalline HAp [34]. An indication of the higher crystallinity is the narrow FWHM. Bands of lower intensities (~ 420 and 580 cm^{-1}) are attributed to other forms of apatites such as octacalcium phosphate and dicalcium phosphate dehydrates [35]. The 1069 cm^{-1} peaks were fixed without shifts for all groups containing TiO_2. This peak has been assigned to apatitic phosphate groups [35], confirming the presence of apatite for all those groups containing TiO_2.

Fig. 3 shows the diffractograms of biomineralized samples. The main peaks (25.9°, 28.9°, 32.1°, 35.6°, and 39.0°) were indexed using JCPDS 72–1243 (hydroxyapatite) and 04–0697 (carbonated apatite) cards [27]. Table 3 shows the crystallite sizes estimated from the most intense peak at the 2θ angle of the XRD reflection according to the Scherrer equation.

The formation of apatite was observed in all analyzed samples. However, obtaining more crystalline apatite is dependent on the surface modification. Clearly, the peaks at 25.9° were more evident and narrower after DLC deposition, independently of TiO_2 concentration. Their

Table 3
Crystallite sizes estimated from the 2θ angle of the most intense peak of XRD reflection.

Sample	Peak (2θ)	Crystallite size (Å)
HAp/Stainless steel	32.08° ± 0.4	103 ± 2.6
HAp/DLC	32.11° ± 0.3	612 ± 2.6
HAp/TiO_2-DLC (0.1 g/L)	32.11° ± 0.2	88 ± 3.6
HAp/TiO_2-DLC (0.3 g/L)	32.02° ± 0.2	103 ± 1.6

Table 2
Results of Gaussian fitting of Raman spectra from DLC and TiO_2-DLC films. $N = 5$.

TiO_2 Concentration (g/L)	*D* Band Position (cm^{-1})	*G* Band Position (cm^{-1})	FWHM (*D*)	FWHM (*G*)	A_D/A_G	$FWHM_D/FWHM_G$
0.0	1330.1 ± 2.3	1531.1 ± 2.6	296.7 ± 0.6	154.2 ± 0.4	0.51 ± 0.04	1.92 ± 0.05
0.1	1354.4 ± 2.7	1552.3 ± 2.4	298.4 ± 0.7	144.9 ± 0.6	0.81 ± 0.02	2.06 ± 0.06
0.3	1349.3 ± 3.3	1537.2 ± 2.1	351.3 ± 0.3	157.9 ± 0.4	0.87 ± 0.03	2.22 ± 0.02

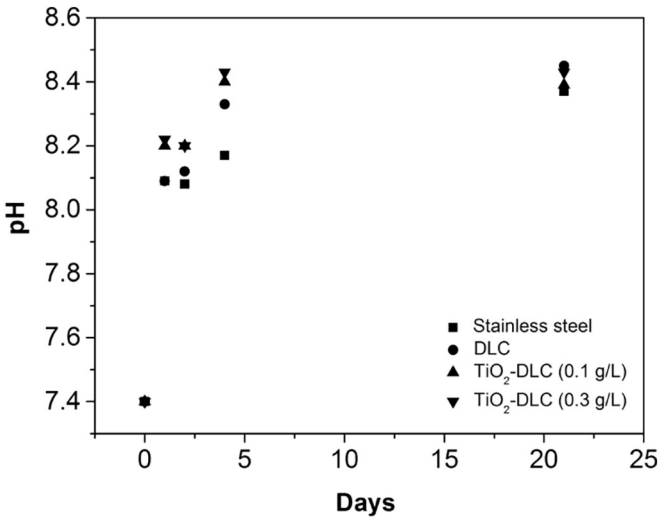

Fig. 4. pH changes of SBF solution versus time due to bioactivity of HAp-composites.

presence is due to sp^2- and sp^3-type C—C bonds. The bioactivity of DLC films has been evaluated when they were incubated in SBF for four months [33,36]. However, those authors observed only the formation of the amorphous phase of apatite, completely differently from what is presented here. However, the great novelty here was the rise in intensity of the XRD peak, which is attributed to the presence of apatite after the incorporation of TiO_2. Interestingly, a decrease in crystallite size was also observed when 0.1 g/L of TiO_2 was incorporated. This probably occurred due to the alignment of the crystalline lattice (also observed by Raman spectra, FWHM G). Contrarily, after the incorporation of three times more TiO_2 (0.3 g/L) nanoparticles, it was not observed. Thus we can infer that an increase in the content of TiO_2 nanoparticles may expose more structural defects, as already observed from the Raman spectra (Fig. 1).

Briefly, we noticed a rapid increase in pH after three days, demonstrating the reactivity of samples when they were soaked in SBF (Fig. 4). It is already reported in the literature that this is a common behavior of bioactive materials, especially bioglass [37]. The increase in the pH values may be related to the release of Ca ions and exchange with H^+ or H_3O^+ ions; this phenomenon occurs on the first day of immersion in the SBF solution, which results in the formation of carbonated HAp.

The contact angles analyzed from drops of distilled water and diiodomethane are shown in Table 4. Clearly, our produced TiO_2-DLC films were hydrophilic and may be associated with the amorphous TiO_2 surfaces [38]. It is known that hydrophilicity is more interesting for biological properties due to protein absorption, cell attachment, and tissue growth [39]. Usually, a hydrophobic surface has a contact angle > 70°, while a hydrophilic surface has a contact angle lower than 70° [40]. Then, the reduction of the contact angle with increases in the concentration of TiO_2 nanoparticles was evidenced (using water, the contact angle decreased from 82° to ~46°). However, this reduction was not observed when diiodomethane was used. We showed that the inclusion of a high concentration of TiO_2 nanoparticles systematically decreased the contact angle of DLC films [24]. It was not possible to measure the water contact angle after the biomineralization because the samples became superhydrophilic ($\theta = 0°$) due to the formation of apatite (as identified in Figs. 2 and 3). This was interesting and had an influence on the identification of the bactericidal properties of produced films.

Usually, a hydrophobic surface has a contact angle higher than 70°, while a hydrophilic surface has one lower than 70° [40]. These results indicate that TiO_2-DLC films are hydrophilic and their hydrophilic characteristic may be attributed to the amorphous TiO_2 surfaces [38].

The surface energy components obtained according to the Owens method [28] are also listed in Table 4. The total surface energy (γ) of 40.0 mN/m for the as-deposited DLC films is estimated as the sum of the dispersive (γ_d = 36.1 mN/m) and polar components (γ_p = 3.6 mN/m). The interfacial free energy determines the wetting characteristics and hence the wall shear stress generated when the liquid comes into contact with the surface [28]. As the concentration of TiO_2 nanoparticles in DLC films increased, the total surface energy also increased from 40.0 to 54.0 mN/m. The rise in the total surface energy of TiO_2-DLC films is attributed to the increase in the polar component (a quantitative indicator of hydrophilicity). It can be directly related to HAp deposition on DLC surfaces when soaked in SBF solution. TiO_2-DLC films have a higher polar component due to the oxide particles on their surfaces [41]. The polar components attract the electric dipoles of water, which minimizes the interfacial energy and the water contact angle [41]. The water contact angle decreased as the polar component in the surface energy increased. The electric dipole of the water molecule is attracted by the polar component, which reduces the interfacial energy between the surface and the water and thus reduces the wetting angle of water [42].

The work of adhesion (W_{Ad}) of HAp crystals in the coatings was calculated using the surface free energy components [43]. According to thermodynamic theory, if W_{Ad} is negative, the adhesion is energetically favorable, whereas if W_{Ad} is positive, the adhesion is thermodynamically unfavorable. Among the coatings, the presence of an increased quantity of TiO_2 nanoparticles in DLC films increased the HAp work of adhesion. This was clearly evidenced by the SEM, Raman, and XRD analyses. Although the DLC films favor HAp deposition (due to the value negative of the adhesion force), we identified a seven-fold increase when compared with the incorporation of 0.3 g/L of TiO_2. It can be related to the negative value of the adhesion force after the inclusion of TiO_2 nanoparticles, which are associated with the hydrophilicity of the DLC films. At the same time, the enhancement of hydrophilicity promoted more deposition of HAp on TiO_2-DLC surfaces compared to DLC. The influence of the adhesion force on cell adhesion, protein adsorption, cell differentiation, and bacteria growth and death has already been systematically reported [44–46]. As far as we know, there are no studies related to the work adhesion force that aim to evaluate HAp deposition using the biomimetic method. Elaborating models to relate Ca and P ions with the adhesion force calculated using polar and non-polar constants from contact angle analysis would be interesting and would open up new perspectives.

Fig. 5 shows SEM micrographs of apatite formation on different samples. Globular apatites were deposited on all the samples. The crystal deposition appears to be more homogeneous when fewer TiO_2 nanoparticles are incorporated. The same occurs with the apatite layer

Table 4
Contact angle and surface energy components of DLC and TiO_2-DLC films with different TiO_2 concentrations. Each mean value corresponds to the average value of five different areas.

Concentration of TiO_2 nanoparticles (g/L)	Contact angle, θ (°)		Surface energy components (mN/m)			Work of adhesion (mJ/m^2)
	Water	Diiodomethane	Dispersive	Polar	Total	
0.0	82.0 ± 4.7	38.5 ± 1.0	36.1 ± 1,5	3.6 ± 1.9	40.0 ± 3.3	−1.03
0.1	72.1 ± 4.7	42.7 ± 1.5	31.1 ± 1.4	9.5 ± 2.8	40.6 ± 4.2	−2.84
0.3	46.0 ± 5.2	42.7 ± 0.2	25.5 ± 0.9	28.5 ± 4.1	54.0 ± 5.0	−7.89

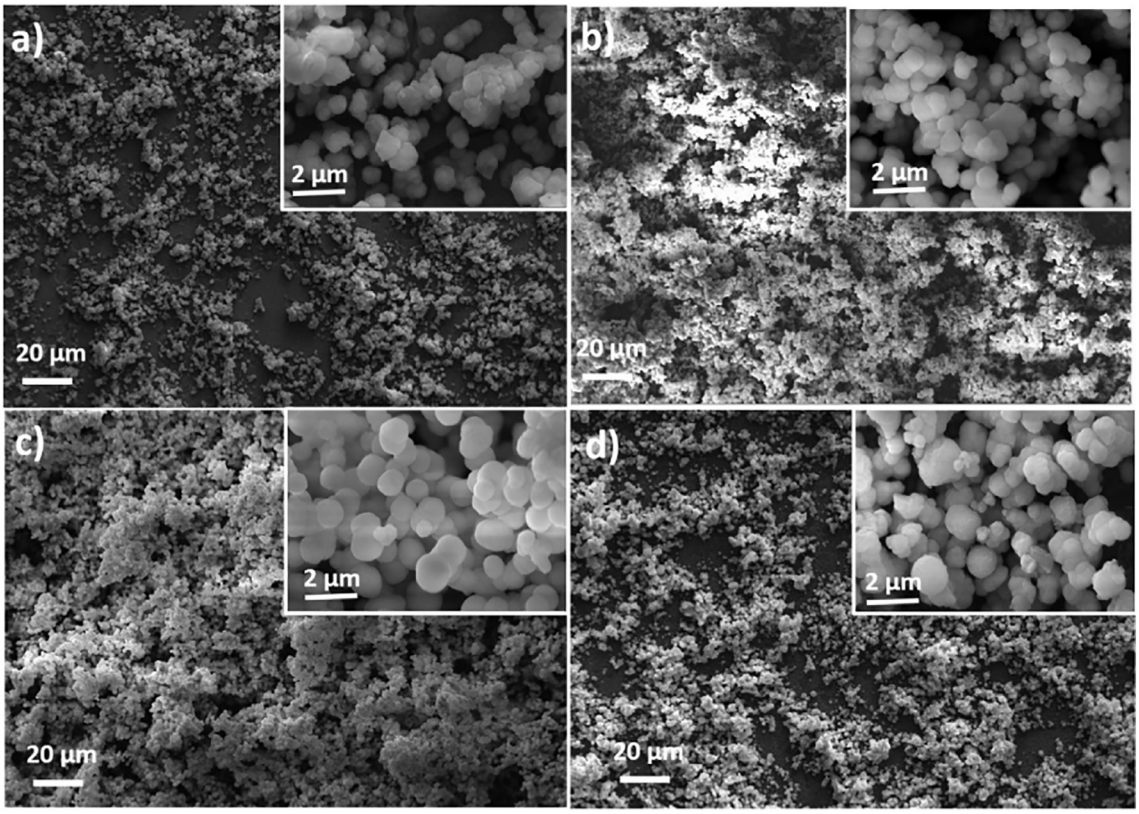

Fig. 5. SEM micrographs of (a) stainless steel, (b) DLC, (c) TiO_2-DLC (0.1 g/L), and (d) TiO_2-DLC (0.3 g/L) surfaces after biomineralization.

densification. The homogeneity of apatite formed can be related to the adhesion force calculated from contact angle analysis. The non-homogeneity of the distribution of diameters may be directly related to the method used to obtain them. The biomimetic method is an interesting way to cover biomaterials surfaces with apatite; however, there are many limitations regarding the control of the size and thickness of the obtained films, as already reported by Kokubo's group [47].

Fig. 6 shows the number of CFUs per milliliter obtained from the HAp/stainless steel, HAp/DLC, and HAp/TiO_2-DLC (0.1 and 0.3 g/L) in microbial biofilms. Briefly, no statistical difference was observed between the stainless steel, DLC, and TiO_2-DLC (0.1 g/L) samples. This can be related to the high standard deviation of the stainless steel

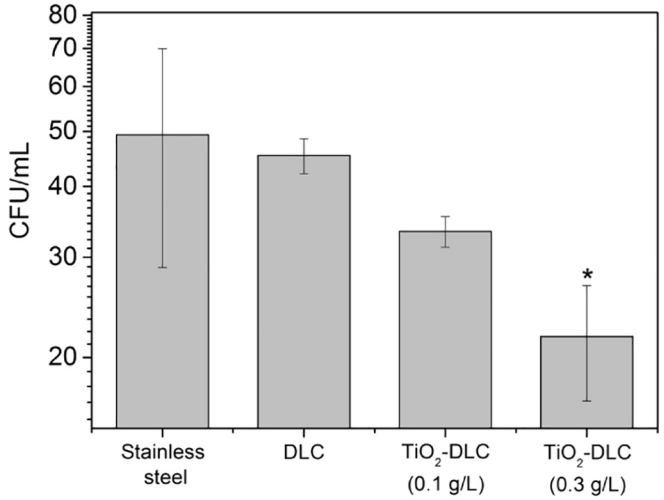

Fig. 6. Number of CFUs per milliliter obtained from HAp-stainless steel, DLC, and TiO_2-DLC films on ATCC strains of *Staphylococcus aureus*. Results are the average ± SD for $n = 5$. * The interaction is considered significant at $P < 0.05$.

(maybe due to the smooth surface of this group). The HAp/TiO_2-DLC (0.3 g/L) films showed significant differences ($p < 0.05$) compared to all the other groups. Again, this can be clearly related to the hydrophilicity, as already explained previously. It was evident that the sevenfolder of hydrophilicity and more homogeneous apatite formation directly influenced the bactericidal properties of DLC-TiO_2 (0.3 g/L). These results are in agreement with those of previously published manuscripts [16,24] reporting on the incorporation of different amounts of TiO^2 and evaluation of their antimicrobial properties. Even though the biofilms may be ten to a thousand times more resistant to an antimicrobial agent [48], because the HAp acts as a synergic agent, enhancing the antimicrobial function of TiO_2.

The bioactivity of biomaterials is the first requirement to define their application to improve bone regeneration. Nevertheless, biomineralization has only partially succeeded in creating high performance composites thus far. Many researchers pay great attention to the mechanism of biomineralization on different material surfaces. On the other hand, microbial biofilms can cause osseous infections, a concept elucidated only in recent decades because of advancements in modern microbiology detection and imaging techniques. Clearly, we cannot seriously consider or elucidate the possibility of direct bone resorption by biofilm pathogens [49]. The microbial biofilm pathogens may induce the inflammatory destruction of HAp as well as its entrapment during osseous infections [49].

Fig. 7 shows a correlation between the work of adhesion of HAp crystals and the number of bacterial colonies in the coatings. The more HAp crystals are adhered to the film surface (Table 4), the less microbial biofilm is adhered on the coating surface (Fig. 6). When HAp is present in TiO_2-DLC surfaces, it spontaneously bonds with bone tissue. However, this relationship with bacteria is still unclear. Some researches [50,51] report that HAp has antibacterial properties, whilst others report that HAp favors the formation of bacterial biofilm. In the present study, TiO_2 nanoparticles increased both the work of adhesion of HAp crystals and the antibacterial activity of TiO_2-DLC surfaces.

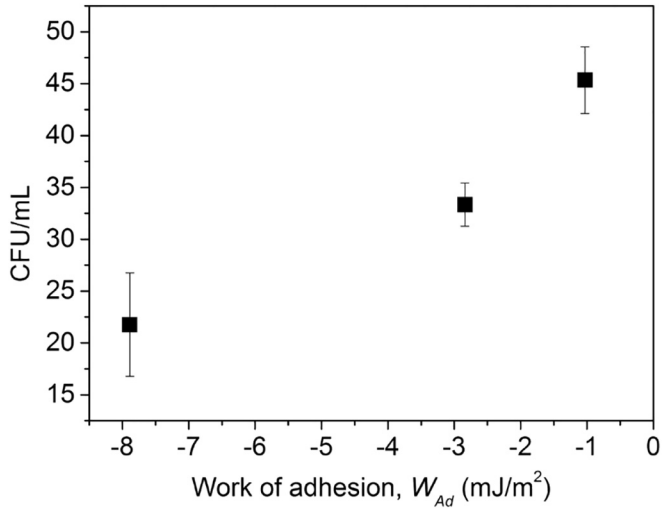

Fig. 7. Number of CFUs per milliliter obtained in HAp/stainless steel, HAp/DLC, and HAp/TiO_2-DLC films on ATCC strains of *Staphylococcus aureus* versus the work of adhesion of HAp crystals in these coatings. Results are the average ± SD for $n = 5$.

4. Conclusion

Herein, the antibacterial properties of HAp/TiO_2-DLC coatings were studied and related to hydrophilicity properties for the first time. We obtained hydroxyapatite (HAp) on DLC films with and without the incorporation of TiO_2 nanoparticles. The presence of TiO_2 nanoparticles increased the graphite-like bonds and decreased the DLC disorder. After biomineralization, the peaks of formed hydroxyapatite and carbonated apatite were indexed by XRD. The Raman spectra of HAp/TiO_2-DLC indicate the characteristics of crystalline HAp and other forms of apatites such as octacalcium phosphate and dicalcium phosphate dehydrates. The presence of an increased number of TiO_2 nanoparticles in the DLC films increased the HAp work of adhesion. The deposited HAp was globular with a spherulitic appearance and were obtained homogenously on all the samples. The HAp/TiO_2-DLC presented an increase in the antibacterial activity of microbial biofilms. This study shows that HAp can work in synergy with TiO_2 to provide an antimicrobial effect against opportunistic pathogens.

Acknowledgments

The authors would like to thank the Sao Paulo Research Foundation (FAPESP, grant nos. 2011/17877-7, 2011/20345-7, 2012/15857-1, 2014/11491-8, 2015/09697-0, and 2016/00575-1), the National Council for Scientific and Technological Development (CNPq grant nos. 310973/2014-7 and 310659/2014-0), Coordination for the Improvement of Higher Education Personnel (CAPES, grant nos. 88881.120138/2016-01 and 88881.120221/2016-01), and Universidade Brasil for the scholarships. Special thanks are owed to Maria Lucia Brison for the SEM micrographs.

References

[1] M.M. Dewidar, K.A. Khalil, J.K. Lim, Processing and mechanical properties of porous 316L stainless steel for biomedical applications, Trans. Nonferrous Metals Soc. China 17 (2007) 468–473.
[2] I. Gurappa, Development of appropriate thickness ceramic coatings on 316 L stainless steel for biomedical applications, Surf. Coat. Technol. 161 (2002) 70–78.
[3] A. Amanov, S.W. Lee, Y.S. Pyun, Low friction and high strength of 316L stainless steel tubing for biomedical applications, Mater. Sci. Eng. C 71 (2017) 176–185.
[4] T. Eliades, H. Pratsinis, D. Kletsas, G. Eliades, M. Makou, Characterization and cytotoxicity of ions released from stainless steel and nickel-titanium orthodontic alloys, Am. J. Orthod. Dentofac. Orthop. 125 (2004) 24–29.
[5] K.-T. Oh, K.-N. Kim, Ion release and cytotoxicity of stainless steel wires, Eur. J. Orthod. 27 (2005) 533–540.
[6] C.-C. Shih, C.-M. Shih, Y.-Y. Su, L.H.J. Su, M.-S. Chang, S.-J. Lin, Effect of surface oxide properties on corrosion resistance of 316L stainless steel for biomedical applications, Corros. Sci. 46 (2004) 427–441.
[7] Q. Tan, J. Ji, M.A. Barbosa, C. Fonseca, J. Shen, Constructing thromboresistant surface on biomedical stainless steel via layer-by-layer deposition anticoagulant, Biomaterials 24 (2003) 4699–4705.
[8] J. Robertson, Diamond-like amorphous carbon, Mater. Sci. Eng. R 37 (2002) 129–281.
[9] C. Donnet, J. Fontaine, T. Le Mogne, M. Belin, C. Heau, J.P. Terrat, F. Vaux, G. Pont, Diamond-like carbon-based functionally gradient coatings for space tribology, Surf. Coat. Technol. 120 (1999) 548–554.
[10] D.Y. Yun, W.S. Choi, Y.S. Park, B. Hong, Effect of H(2) and O(2) plasma etching treatment on the surface of diamond-like carbon thin film, Appl. Surf. Sci. 254 (2008) 7925–7928.
[11] A. Shirakura, M. Nakaya, Y. Koga, H. Kodama, T. Hasebe, T. Suzuki, Diamond-like carbon films for PET bottles and medical applications, Thin Solid Films 494 (2006) 84–91.
[12] C. Anandan, L. Mohan, P.D. Babu, Electrochemical studies and growth of apatite on molybdenum doped DLC coatings on titanium alloy β-21S, Appl. Surf. Sci. 296 (2014) 86–94.
[13] T. Yokota, T. Terai, T. Kobayashi, T. Meguro, M. Iwaki, Cell adhesion to nitrogen-doped DLCs fabricated by plasma-based ion implantation and deposition method using toluene gas, Surf. Coat. Technol. 201 (2007) 8048–8051.
[14] E. Eisenbarth, D. Velten, K. Schenk-Meuser, P. Linez, V. Biehl, H. Duschner, J. Breme, H. Hildebrand, Interactions between cells and titanium surfaces, Biomol. Eng. 19 (2002) 243–249.
[15] H. Nakano, N. Hasuike, K. Kisoda, K. Nishio, T. Isshiki, H. Harima, Synthesis of TiO2 nanocrystals controlled by means of the size of magnetic elements and the level of doping with them, J. Phys. Condens. Matter (2009) 21.
[16] P.C. Maness, S. Smolinski, D.M. Blake, Z. Huang, E.J. Wolfrum, W.A. Jacoby, Bactericidal activity of photocatalytic TiO_2 reaction: toward an understanding of its killing mechanism, Appl. Environ. Microbiol. 65 (1999) 4094–4098.
[17] A. Afkhami, A. Shirzadmehr, T. Madrakian, Improvement in performance of a hyoscine butylbromide potentiometric sensor using a new nanocomposite carbon paste: a comparison study with polymeric membrane sensor, Ionics 20 (2014) 1145–1154.
[18] H. Bagheri, A. Afkhami, A. Shirzadmehr, H. Khoshsafar, A new nano-composite modified carbon paste electrode as a high performance potentiometric sensor for nanomolar Tl(I) determination, J. Mol. Liq. 197 (2014) 52–57.
[19] E. Ye, X.J. Loh, Polymeric hydrogels and nanoparticles: a merging and emerging field, Aust. J. Chem. 66 (2013) 997–1007.
[20] X.J. Loh, T.-C. Lee, Q. Dou, G.R. Deen, Utilising inorganic nanocarriers for gene delivery, Biomater. Sci. 4 (2016) 70–86.
[21] E. Ye, M.D. Regulacio, M.S. Bharathi, H. Pan, M. Lin, M. Bosman, K.Y. Win, H. Ramanarayan, S.-Y. Zhang, X.J. Loh, Y.-W. Zhang, M.-Y. Han, An experimental and theoretical investigation of the anisotropic branching in gold nanocrosses, Nano 8 (2016) 543–552.
[22] H.C. Guo, E. Ye, Z. Li, M.-Y. Han, X.J. Loh, Recent progress of atomic layer deposition on polymeric materials, Mater. Sci. Eng. C 70 (Part 2) (2017) 1182–1191.
[23] Z. Li, E. Ye, R. Lakshminarayanan David, X.J. Loh, Recent advances of using hybrid nanocarriers in remotely controlled therapeutic delivery, Small 12 (2016) 4782–4806.
[24] F.R. Marciano, D.A. Lima-Oliveira, N.S. Da-Silva, A.V. Diniz, E.J. Corat, V.J. Trava-Airoldi, Antibacterial activity of DLC films containing TiO_2 nanoparticles, J. Colloid Interface Sci. 340 (2009) 87–92.
[25] G. Thorwarth, B. Saldamli, F. Schwarz, P. Jurgens, C. Leiggener, R. Sader, M. Haeberlen, W. Assmann, B. Stritzker, Biocompatibility of doped diamond-like carbon coatings for medical implants, Plasma Process. Polym. 4 (2007) S364–S368.
[26] M.S. Amin, L.K. Randeniya, A. Bendavid, P.J. Martin, E.W. Preston, Biomimetic apatite growth from simulated body fluid on various oxide containing DLC thin films, Diam. Relat. Mater. 21 (2012) 42–49.
[27] F. Barrere, M.M.E. Snel, C.A. van Blitterswijk, K. de Groot, P. Layrolle, Nano-scale study of the nucleation and growth of calcium phosphate coating on titanium implants, Biomaterials 25 (2004) 2901–2910.
[28] D.K. Owens, R.C. Wendt, Estimation of surface free energy of polymers, J. Appl. Polym. Sci. 13 (1969) (1741- &).
[29] R.E. Neuendorf, E. Saiz, A.P. Tomsia, R.O. Ritchie, Adhesion between biodegradable polymers and hydroxyapatite: relevance to synthetic bone-like materials and tissue engineering scaffolds, Acta Biomater. 4 (2008) 1288–1296.
[30] A.W. Adamson, The physical chemistry of surfaces, Abstr. Pap. Am. Chem. Soc. 221 (2001) (U320-U320).
[31] A.C. Ferrari, J. Robertson, Raman spectroscopy of amorphous, nanostructured, diamond–like carbon, and nanodiamond, Philos. Trans. R. Soc. London, Ser. A 362 (2004) 2477–2512.
[32] J. Robertson, Diamond-like amorphous carbon, Mater. Sci. Eng. R. Rep. 37 (2002) 129–281.
[33] M.S. Amin, L.K. Randeniya, A. Bendavid, P.J. Martin, E.W. Preston, Amorphous carbonated apatite formation on diamond-like carbon containing titanium oxide, Diam. Relat. Mater. 18 (2009) 1139–1144.
[34] S. Kale, S. Biermann, C. Edwards, C. Tarnowski, M. Morris, M.W. Long, Three-dimensional cellular development is essential for ex vivo formation of human bone, Nat. Biotechnol. 18 (2000) 954–958.
[35] T.C.O. Marsi, T.G. Santos, C. Pacheco-Soares, E.J. Corat, F.R. Marciano, A.O. Lobo, Biomineralization of Superhydrophilic vertically aligned carbon nanotubes, Langmuir 28 (2012) 4413–4424.
[36] J. Kunze, L. Müller, J.M. Macak, P. Greil, P. Schmuki, F.A. Müller, Time-dependent growth of biomimetic apatite on anodic TiO_2 nanotubes, Electrochim. Acta 53

(2008) 6995–7003.
[37] Z.H. Zhou, J.M. Ruan, J.P. Zou, Z.C. Zhou, X.J. Shen, Bioactivity of bioresorbable composite based on bioactive glass and poly-L-lactide, Trans. Nonferrous Metals Soc. China 17 (2007) 394–399.
[38] A. Sobczyk-Guzenda, M. Gazicki-Lipman, H. Szymanowski, J. Kowalski, P. Wojciechowski, T. Halamus, A. Tracz, Characterization of thin TiO_2 films prepared by plasma enhanced chemical vapour deposition for optical and photocatalytic applications, Thin Solid Films 517 (2009) 5409–5414.
[39] P. Roach, D. Eglin, K. Rohde, C.C. Perry, Modern biomaterials: a review—bulk properties and implications of surface modifications, J. Mater. Sci. Mater. Med. 18 (2007) 1263–1277.
[40] H.W. Choi, R.H. Dauskardt, S.C. Lee, K.R. Lee, K.H. Oh, Characteristic of silver doped DLC films on surface properties and protein adsorption, Diam. Relat. Mater. 17 (2008) 252–257.
[41] R.K. Roy, H.W. Choi, J.W. Yi, M.W. Moon, K.R. Lee, D.K. Han, J.H. Shin, A. Kamijo, T. Hasebe, Hemocompatibility of surface-modified, silicon-incorporated, diamond-like carbon films, Acta Biomater. 5 (2009) 249–256.
[42] R.K. Roy, H.W. Choi, S.J. Park, K.R. Lee, Surface energy of the plasma treated Si incorporated diamond-like carbon films, Diam. Relat. Mater. 16 (2007) 1732–1738.
[43] M.P. Ferraz, F.J. Monteiro, A.P. Serro, B. Saramago, I.R. Gibson, J.D. Santos, Effect of chemical composition on hydrophobicity and zeta potential of plasma sprayed HA/CaO-P2O5 glass coatings, Biomaterials 22 (2001) 3105–3112.
[44] L.-C. Xu, C.A. Siedlecki, Effects of surface wettability and contact time on protein adhesion to biomaterial surfaces, Biomaterials 28 (2007) 3273–3283.
[45] T.J. Webster, R.W. Siegel, R. Bizios, Osteoblast adhesion on nanophase ceramics, Biomaterials 20 (1999) 1221–1227.
[46] Y.-L. Ong, A. Razatos, G. Georgiou, M.M. Sharma, Adhesion forces between *E. coli* bacteria and biomaterial surfaces, Langmuir 15 (1999) 2719–2725.
[47] T. Kokubo, Apatite formation on surfaces of ceramics, metals and polymers in body environment, Acta Mater. 46 (1998) 2519–2527.
[48] J.R. de Oliveira, R.B. de Aguiar Almeida, P. das Gracas Figueiredo Vilela, F.E. de Oliveira, R.F. da Rocha, A.O. Jorge, L.D. de Oliveira, Control of microorganisms of oral health interest with *Arctium lappa* L. (burdock) extract non-cytotoxic to cell culture of macrophages (RAW 264.7), Arch. Oral Biol. 59 (2014) 808–814.
[49] G.D. Ehrlich, P. Stoodley, S. Kathju, Y.J. Zhao, B.R. McLeod, N. Balaban, F.Z. Hu, N.G. Sotereanos, J.W. Costerton, P.S. Stewart, J.C. Post, Q. Lin, Engineering approaches for the detection and control of orthopaedic biofilm infections, Clin. Orthop. Relat. Res. (2005) 59–66, http://dx.doi.org/10.1097/01.blo.0000175125.60214.a4.
[50] J. Hasan, R.J. Crawford, E.P. Lvanova, Antibacterial surfaces: the quest for a new generation of biomaterials, Trends Biotechnol. 31 (2013) 31–40.
[51] A. Murakami, T. Arimoto, D. Suzuki, M. Iwai-Yoshida, F. Otsuka, Y. Shibata, T. Igarashi, R. Kamijo, T. Miyazaki, Antimicrobial and osteogenic properties of a hydrophilic-modified nanoscale hydroxyapatite coating on titanium, Nanomedicine 8 (2012) 374–382.